2016

Synthesis, Structure, and Properties of Al(Rbpy)3 Complexes (R = tBu, Me): Homoleptic Main-Group Tris-bipyridyl Compounds

DeCarlo, Samantha; Dennis H. Mayo; Warren Tomlinson; Junkai Hu; Hooper, Joseph; Peter Zavalij; Kit Bowen; Hansgeorg Schnockel; Bryan Eichhorn

DeCarlo, Samantha, et al. "Synthesis, Structure, and Properties of Al (Rbpy) 3 Complexes (R= t-Bu, Me): Homoleptic Main-Group Tris-bipyridyl Compounds." Inorganic chemistry (2016), 55, 4344-4353.
https://hdl.handle.net/10945/48738

Inorganic Chemistry

Article

pubs.acs.org/IC

Synthesis, Structure, and Properties of Al(^{R}bpy)$_3$ Complexes (R = *t*-Bu, Me): Homoleptic Main-Group Tris-bipyridyl Compounds

Samantha DeCarlo,[†] Dennis H. Mayo,[†,§] Warren Tomlinson,[⊥] Junkai Hu,[†] Joseph Hooper,[⊥] Peter Zavalij,[†] Kit Bowen,[‡] Hansgeorg Schnöckel,[∥] and Bryan Eichhorn*[,†]

[†]Department of Chemistry and Biochemistry University of Maryland—College Park, College Park, Maryland 20742, United States
[‡]Departments of Chemistry and Materials Science Johns Hopkins University, Baltimore, Maryland 21218, United States
[§]Research Department Naval Surface Warfare Center Indian Head EOD Tech Division, Indian Head, Maryland 20640, United States
[∥]Institute of Inorganic Chemistry, Karlsruhe Institute of Technology (KIT), D-76128 Karlsruhe, Germany
[⊥]Department of Physics, Naval Postgraduate School, Monterey, California 93943, United States

Supporting Information

ABSTRACT: The neutral homoleptic tris-bpy aluminum complexes Al(^{R}bpy)$_3$, where R = tBu (**1**) or Me (**2**), have been synthesized from reactions between AlX precursors (X = Cl, Br) and neutral ^{R}bpy ligands through an aluminum disproportion process. The crystalline compounds have been characterized by single-crystal X-ray diffraction, electrochemical experiments, EPR, magnetic susceptibility, and density functional theory (DFT) studies. The collective data show that **1** and **2** contain Al^{3+} metal centers coordinated by three bipyridine $(bpy^{\bullet})^{1-}$ monoanion radicals. Electrochemical studies show that six redox states are accessible from the neutral complexes, three oxidative and three reductive, that involve oxidation or reduction of the coordinated bpy ligands to give neutral ^{R}bpy or ^{R}bpy^{2-} dianions, respectively. Magnetic susceptibility measurements (4–300 K) coupled with DFT studies show strong antiferromagnetic coupling of the three unpaired electrons located on the ^{R}bpy ligands to give $S = {}^{1}/_{2}$ ground states with low lying $S = {}^{3}/_{2}$ excited states that are populated above 110 K (**1**) and 80 K (**2**) in the solid-state. Complex **2** shows weak 3D magnetic interactions at 19 K, which is not observed in **1** or the related [Al(bpy)$_3$] complex.

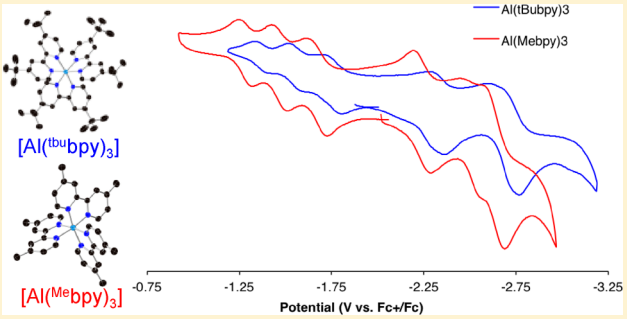

INTRODUCTION

The 2,2′-bipyridine (bpy) ligand and its derivatives are some of the most commonly used bidentate nitrogen donor ligands in coordination chemistry (Figure 1a). Widespread use of bipyridine ligands stems from their commercial availability and propensity to form stable 5-member chelate rings by coordinating in an N,N′ fashion to main-group, transition, and f-block metals.[1] In the past 50+ years, bpy coordination complexes have been extensively studied, including $[M(bpy)_3]^n$ homoleptic tris-bpy complexes (M = transition metal, $n = -3$ to $+3$)[2−5] such as the well-known $[Ru(bpy)_3]^n$ series.[2,6] Interest in these complexes arises from their propensity to form helical assemblies and luminescent devices, their chiral molecular recognition properties, and unique electrochemical behavior that is often characterized by multiple accessible oxidation states.[1] The redox-active nature of the bpy ligand can give rise to ligand-centered radicals that couple with each other or to a magnetic metal center, resulting in interesting magnetic and electronic properties.

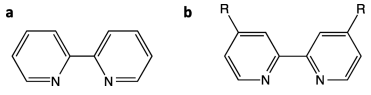

Figure 1. (a) 2,2′-Bipyridine, bpy, ($C_{10}H_8N_2$). (b) 4,4′-di-R-2,2′-bipyridine, ^{R}bpy.

There are numerous examples of neutral homoleptic tris-bpy complexes containing the parent 2,2′-bipyridine ligand (Figure 1a) with various metals and ligand oxidation states (see Table 1), although few have been structurally characterized. However, several homoleptic tris-bpy metal complexes containing the 4,4′-substituted bpy ligands, $R_2C_{10}H_6N_2$ (^{R}bpy where R= Me_2 or $^{t}Bu_2$, Figure 1b), have been synthesized and crystallographically characterized (see Table 2).

In contrast to the large number of transition-metal tris-bpy complexes, there are few examples of main-group metal tris-bipyridine complexes reported in the literature. The first example of a structurally characterized group 13 homoleptic tris-bpy complex, $[Ga(bpy)_3]^{3+}$, was first described by Jones et al. in 2004.[7] More recently, the $[Ga(bpy)_3]^{2+}$ complex was

Received: January 13, 2016
Published: April 11, 2016

DOI: 10.1021/acs.inorgchem.6b00034
Inorg. Chem. 2016, 55, 4344−4353

Table 1. Neutral M(bpy)$_3$ Complexes[a]

complex[b,c]	structurally characterized?	ref
$[Al^{III}(bpy^{\bullet})_3]^0$	no	17
$[Mg^{II}(bpy^{\bullet})_2(bpy^0)]^0$	no	20
$[Sc^{III}(bpy^{\bullet})_3]^0$	no	9
$[Y^{III}(bpy^{\bullet})_3]^0$	no	21
$[Ti^{III}(bpy^{\bullet})_3]^0$	yes	22, 23
$[Zr^{IV}(bpy^{\bullet})_2(bpy^{2-})]^0$	no	24
$[Hf^{IV}(bpy^{\bullet})_2(bpy^{2-})]^0$	no	25
$[V^{II}(bpy^{\bullet})_3(bpy^0)]^0$	no	26
$[Nb^{IV}(bpy^{2-})_2(bpy^0)]^0$	no	21
$[Ta^{V}(bpy^{\bullet})\ (bpy^{2-})_2]^0$	no	25
$[Cr^{III}(bpy^{\bullet})_3]^0$	no	27
$[Mo^{III}(bpy^{\bullet})_3]^0$	no	28
$[Mn^{II}(bpy^{\bullet})_2(bpy^0)]^0$	no	28
$[Re(bpy)_3]^0$	no	25
$[Fe^{II}(bpy^{\bullet})_2(bpy^0)]^0$	no	29, 30
$[Ru^{II}(bpy^{\bullet})_2(bpy^0)]^0$	yes	2
$[Os(bpy^{\bullet})_2(bpy^0)]^0$	no	2
$[Co(bpy)_3]^0$	no	31

[a]Data from ref 15. [b]bpy = $C_{10}N_2H_8$; bpy$^{\bullet}$ = $[C_{10}N_2H_8]^-$. [c]Oxidation states assigned by refs 5, 16−18.

Table 2. Select Examples of 4,4′-Disubstituted Homoleptic Tris-bpy Complexes

complex	ref
$[Ti(^{Me}bpy)_3]^0$	5
$[V(^{Me}bpy)_3]^0$	5
$[Fe(^{tBu}bpy)_3]^{2+}$	32
$[Mo(^{Me}bpy)_3]^0$	33
$[Cr(^{Me}bpy)_3]^0$	5
$[V(^{tBu}bpy)]^n$ (n = 3+, 2+, 0, 1−)	4
$[Fe(dmbpy)]^{2+}$ (dmbpy = 5,5′-dimethyl-2,2′-bipyridyl)	34
$[Mo(^{tBu}bpy)_3]^{2+}$	35
$[Co(^{Me}bpy)_3]^{2+}$	36, 37
$[Fe(^{Me}bpy)_3]^{2+}$	38
$[Ru(dcmbbpy)_3]^{2+}$ (dcmb = 4,4′-dimethyl-2,2′-bipyridine)	39
$[Ru(^{tBu}bpy)_3]^{2+}$	39,40
$[Zn(tmamb)_3]^{2+}$ (tmamb = 4,4-triethylaminomethyl-2,2′-bipyridine)	41
$[Fe(dabp)_3]2+$ (dabp = 5,5′-diamino-2,2′-bipyridine)	42
$[Ru(^{Me}bpy)_3]^{2+}$	43
$[Ru(dmesb)_3]^{2+}$ (dmesb =4,4′-dimesityl-2,2′-bipyridine)	44
$[Ru(dadcb)_3]^{2+}$ (dadcb = *N*,*N*′-diallyl-4,4′-dicarboxamide-2,2′-bipyridyl)	45
$[Zn(homb)_3]^{2+}$ (homd = 4,4′-bis(hydroxymethyl)-2,2′-bipyridine)	46
$[Zn(mob)_3]^{2+}$ (mob = 4,4′-bis(methoxy)-2,2′-bipyridine)	46

isolated and characterized.[8] Both complexes contain Ga^{3+} metal ions, where the latter complex contains two neutral bpy ligands and one radical bpy anion as discussed below. Group 3 $[Sc(bpy)_3]^0$ and group 14 $[Si(bpy)_3]^n$ (where n = 4+ to 1+) have been described but not structurally characterized.[9−11] One heptacoordinate tris-bpy complex of thallium (Tl(bpy)$_3$dmso, dmso = dimethylsulfoxane) has been prepared and crystallographically characterized, but it contains an additional dmso ligand in the Tl coordination sphere.[12] Although there is a lack of main-group homoleptic tris bpy complexes, other redox-active bidentate N-donor ligands have been structurally characterized containing aluminum centers.[13] In particular, the synthesis and characterization of $[Al(dpt)_3]$ (dpt = 1,3-dipehnyltrianzenido) demonstrates the unusual electrochemical properties of these systems and the viability of isolating the radical anion complexes such as $[Al(dpt)_3]^-$.[14,15]

Homoleptic aluminum tris-bpy, Al(bpy)$_3$, has been synthesized in polycrystalline form and characterized through DFT calculations and magnetometry, but the crystal structure has not been reported.[16−18] While the initial reports of the neutral Al(bpy)$_3$ complex were mostly compositional in nature,[17] subsequent computational and spectroscopic studies indicate that the complex contains an Al^{3+} center coordinated by three monoanionic bpy ([bpy$^{\bullet}$]$^-$) ligands.[16,18] DFT calculations suggest a symmetrical D_3 structure with an $S = {}^1/_2$ ground state and an $S = {}^3/_2$ excited state that is only slightly higher in energy. This finding is in support of magnetometry experiments showing three unpaired electrons in the room temperature susceptibility.[16]

Wieghardt et al. have performed extensive studies of many structurally characterized homoleptic tris-bpy complexes and delineated the important diagnostic role that the C1−C1′ intrachelate bonds have in identifying the redox states of the bpy ligands in these complexes.[1,3] The C1−C1′ bond length can be used to differentiate between neutral, monoanionic, and dianionic bpy ligands (Scheme 1), which can then be used to determine the oxidation state of the metal center. This analysis is applicable to both substituted and nonsubstituted bpy ligands.[3,5,18]

Scheme 1. Bpy Oxidation States and Relevant Bond Distances[a,b]

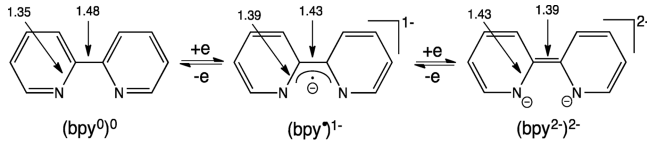

[a]Distances in Å, with ∼±0.01 Å. [b]Adapted with permission from ref 18. Copyright American Chemical Society 2013.

Because there are very few structurally characterized main-group bpy complexes, experimental studies that employ this analysis have been primarily focused on transition-metal bpy complexes. A recent DFT study of group 14 metal complexes suggests that analogous bond length trends should also be exhibited in main-group bpy systems.[10]

There is little data correlating structural and physical properties of the main-group $[M(bpy)_3]^n$ complexes, and their relationships to the transition-metal complexes remain to be established. Here we describe the synthesis and characterization of the first structurally characterized aluminum homoleptic tris-bpy complexes $[Al(^{tBu}bpy)_3]$ (**1**) and $[Al(^{Me}bpy)_3]$ (**2**). Both of these complexes were synthesized through the use of an aluminum monohalide (AlX) precursor solution.[19] Structural, electrochemical, electrospray ionization mass spectrometry (ESI-MS), magnetometry, and theoretical studies have been performed on both **1** and **2** and are described in detail. These studies show that the substituted bpy ligands in **1** and **2** are monoanionic radical anions, $(^{R}bpy^{\bullet})^{1-}$, with both complexes containing Al^{3+} ions. Electrochemical experiments coupled with DFT calculations demonstrate that the three free electrons in the system are ligand-based. Magnetometry experiments show that the free electrons in the complexes are antiferromagnetically coupled yielding $S = {}^1/_2$ ground states, in solution at room temperature, with low lying $S = {}^3/_2$ excited states, observed at room temperature in the solid-state.

DOI: 10.1021/acs.inorgchem.6b00034
Inorg. Chem. 2016, 55, 4344−4353

Magnetometry further shows that complex **2** has unusual 3D antiferromagnetic interactions below 80 K in the solid-state.

RESULTS

Synthesis. The neutral tris-bpy complexes Al(^{tBu}bpy)$_3$] (**1**) and [Al(^{Me}bpy)$_3$] (**2**) were synthesized by a reaction of AlBr·(NEt$_3$)$_n$ with 1 equiv of ^{R}bpy (R = tBu or Me) in THF at room temperature. Both **1** and **2** form in approximately 35% total yield comprising black needle-like crystals (~10%) and black polycrystalline powders (~25%) that have been characterized via powder X-ray diffraction (Figure S1). In addition, Al metal deposits on the walls of the reaction vessel during the synthesis. Complex **1** can also be prepared in similar yield from the reaction of AlCl·(Et$_2$O)$_n$ and ^{R}bpy.

The reactions presumably occur through disproportionation of the AlBr precursor during ligand metathesis as shown in eq 1.

$$3\mathrm{AlBr} + 3\,^{R}\mathrm{bpy} \xrightarrow{\mathrm{THF}} [\mathrm{Al}(^{R}\mathrm{bpy})_3]^0 + \mathrm{AlBr_3} + \mathrm{Al}^0 \qquad \mathrm{R} = {}^{t}\mathrm{Bu},\ \mathrm{Me} \qquad (1)$$

Single crystals of these complexes suitable for X-ray crystallography were grown at room temperature in the concentrated reaction mixture. The crystals of both **1** and **2** are soluble in THF and CH$_3$CN. Both complexes are air- and moisture-sensitive in solution and the solid-state and have been characterized by single-crystal X-ray diffraction, X-ray powder diffraction, EPR, dc magnetic susceptibility, electrochemistry, and electrospray ionization mass spectrometry (ESI-MS) and DFT studies.

Solid-State Structures. Both [Al(^{tBu}bpy)$_3$] (**1**) and [Al(^{Me}bpy)$_3$] (**2**) form black needle-like crystals. Summaries of the crystal data are given in Table S1, and selected bond distances and angles are reported in Tables 3 and 4. ORTEP drawings of the complexes are given in Figures 2 and 3.

Table 3. Selected Bond Lengths (Å) and Angles (deg) for Al(^{tBu}bpy)$_3$ (1)

Al1−N10	1.995(6)	N10−Al1−N20	78.66(18)
N10−C15	1.363(8)	C15−N10−Al1	116.9(6)
C14−C15	1.416(4)	C11−N10−Al1	124.0(4)
C15−C21	1.420(5)	C21−N20−Al1	116.2(6)
N20−C21	1.368(8)	N10−Al1−N10	97.1(6)
C24−C25	1.379(4)	N20−Al1−N20	96.5(6)
Al1−N20	1.997(6)	N10−Al1−N10	82.9(6)
N10−C11	1.365(8)		
C13−C16	1.548(5)		
C16−C19	1.523(6)		
C16−C17	1.530(6)		
N20−C25	1.356(8)		

The structures of **1** and **2** are quite similar, both possessing aluminum atoms coordinated in slightly distorted octahedral environments.[5] Both have virtual D_3 point symmetry. **2** is isomorphic with [Cr(^{Me}bpy)]^0 (Table S2).[5]

The Al−N bond distances in **1** and **2** are slightly shorter than those involving neutral bpy ligands bound to Al^{3+} that are typically in the range 2.03−2.07 Å.[47,48] The shorter bonds to the (^{R}bpy$^{\bullet}$)$^{1-}$ ligands are consistent with the trend observed in [Cr(^{tBu}bpy)$_3$]$^{n+}$ series, where n = 3, 2, and 1, containing both neutral and anionic bpy ligands.[49]

Table 4. Selected Bond Lengths (Å) and Angles (deg) for Al(^{Me}bpy)$_3$ (2)

Al1−N1	2.0002(12)	N1−Al1−N1	80.78(7)
N1−C1	1.3528(18)	N1−Al1−N1	171.90(7)
C1−C2	1.368(2)	N1−Al1−N1	92.58(7)
C2−C3	1.418(2)	N1−Al1−N1	93.59(4)
C3−C4	1.373(2)		
C4−C5	1.417(2)		
C5−C5	1.423(3)		
N1−C5	1.3902(18)		
C1−H1	0.970(17)		
C2−H2	0.978(16)		
C3−C6	1.504(2)		

In the solid-state, the ^{Me}bpy rings of **2** pack with parallel offset π-stacking of the bpy ligands from neighboring molecules. In this structure, the methyl group (C6) is located directly above the centroid of an adjacent right with C6··· centroid distance of 3.701 Å (Figure 4).[50]

This type of π-stacking is also present in the isomorphic [Cr(^{Me}bpy)$_3$] complex and the isostructural monoclinic analogues [Ti(^{Me}bpy)$_3$] and [Mo(^{Me}bpy)$_3$] and is reminiscent of that observed in solid-state toluene.[5,50,51] For these complexes the methyl C···centroid distances are 3.582, 3.515, and 3.765 Å, respectively.[5] The similarities of these interactions among the four compounds suggest that π-stacking has a significant influence in the stability of the crystal lattices regardless of the central metal and the crystal symmetry. Similar interactions are not observed in **1** or other ^{tBu}bpy complexes, presumably due to the sterics associated with the *tert*-butyl groups and general packing within the unit cell.

The polycrystalline precipitates that form along with crystals of **1** and **2** were characterized by powder X-ray diffraction (Figure S1). Comparisons of the experimental and simulated diffraction patterns show that the precipitates are isostructural to the crystalline samples.

Mass Spectrometry. A representative positive ion ESI-MS spectrum of **1** is shown in Figure 5. The parent ion [Al(^{tBu}bpy)$_3$]$^+$ is observed at 832.17 m/z with additional peaks representing [Al(^{tBu}bpy)$_2$]$^+$ and [Al(^{tBu}bpy)]$^+$ fragments at 563.77 and 295.38 m/z, respectively, at much lower intensity. Peaks representing [Al(^{tBu}bpy)$_2$]$^{2+}$, at 418.16 m/z, and the [Al(^{tBu}bpy)$_3$]·THF solvate at 904.28 m/z are also observed. Similar species are observed in the positive ion ESI-MS spectrum of **2** (Figure S2).

Electrochemistry. The cyclic voltammograms (CVs) and square wave voltammograms (SWVs) of **1** and **2** were recorded at ambient temperature in CH$_3$CN solutions containing 0.1 M [N(n-Bu)$_4$]PF$_6$ as the supporting electrolyte. The three-electrode setup contained a glassy carbon working electrode, a platinum counter electrode, and a silver wire pseudoreference electrode. Control experiments of free ligand, solvent, and electrolyte solution were recorded under the same conditions. The CVs and SWVs are shown in Figure 6, and the potentials ($E_{1/2}$) of the redox couples are listed in Table 5. All potentials are referenced to ferrocenium/ferrocene couple Fc$^+$/Fc. Evans method NMR, ESI-MS, and EPR studies (see next section) show that the complexes remain in the neutral, [Al^{3+}(^{R}bpy$^{\bullet}$)$_3$] state prior to electrochemical analysis. The free ^{tBu}bpy ligand in CH$_3$CN shows a quasireversible reduction at −2.71 V and an irreversible oxidation at −1.68 V (see Figure S3). For ^{Me}bpy there is quasireversible reduction at −2.75 V and an irreversible

DOI: 10.1021/acs.inorgchem.6b00034
Inorg. Chem. 2016, 55, 4344−4353

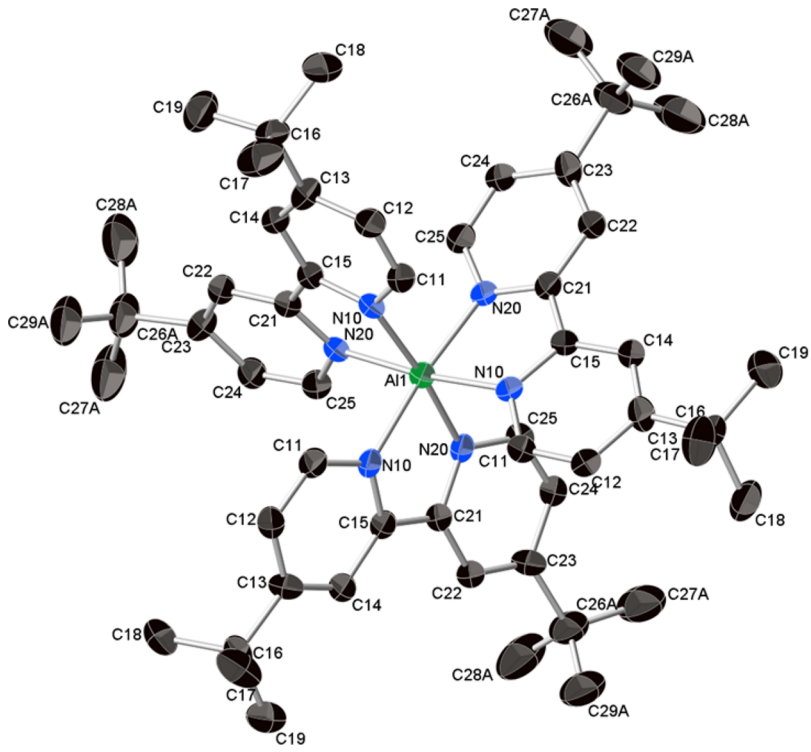

Figure 2. X-ray structure of the neutral complex [Al(^{tBu}bpy)$_3$], **1**. Thermal ellipsoids drawn at the 50% probability level. Hydrogen atoms have been omitted for clarity.

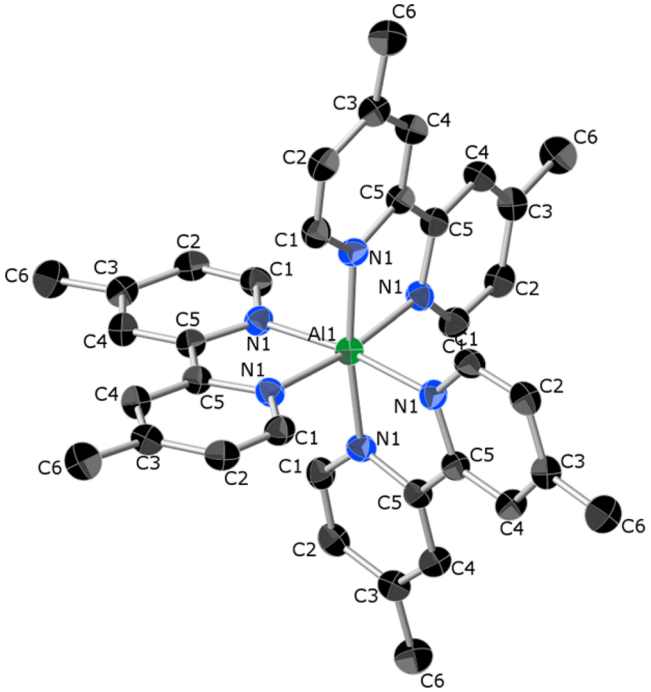

Figure 3. Crystal structure of the [Al(^{Me}bpy)$_3$] complex **2**. Thermal ellipsoids drawn at the 50% probability level. Hydrogen atoms have been omitted for clarity.

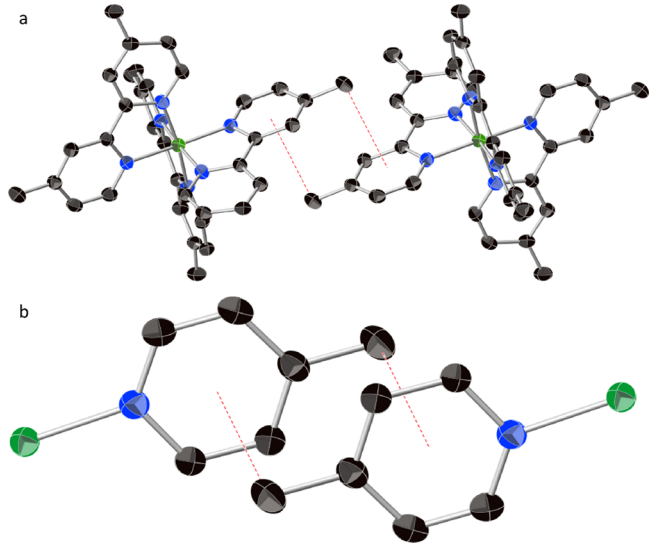

Figure 4. Me−π interactions (red dotted line) of 3.61 Å between two adjacent "chains" of [Al(^{Me}bpy)$_3$] within the crystal lattice. (a) View down [111]. (b) Zoomed in view of interaction between C_{Me} and the neighboring ligand (Me−π) (Al = green; N = blue; C = black; H atoms omitted for clarity).

oxidation at −1.66 V. These redox potentials are distinct from those of **1** and **2**, indicating the absence of free ligands in solutions of the complexes.

The CVs of both **1** and **2** show two distinct regions of waves. The CV curve of **1** (open circuit potential = −2.05 V) exhibits three reversible oxidations at −1.37, −1.56, and −1.76 V (Figure 6a); two quasireversible reductions at −2.31 and −2.67 V; and a nonreversible reduction at −2.99 V. For **2** (rest potential = −2.01 V), a similar pattern exists at slightly more positive values: three reversible oxidations occur for **2** at −1.29, −1.47, −1.68 V (Figure 6a), and three quasireversible reductions occur at −2.24, −2.50, and −2.64 V. The $E_{1/2}$ values for **1** are slightly more negative than observed for complex **2** due to the greater electron donating of the 4,4′-di-*tert*-butyl ligands relative to 4,4′-dimethyl-bpy. The separations

DOI: 10.1021/acs.inorgchem.6b00034
Inorg. Chem. 2016, 55, 4344−4353

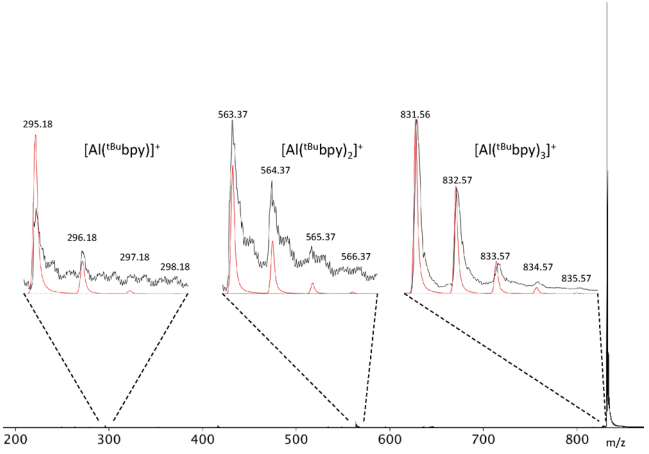

Figure 5. Positive ion ESI-MS of $[Al(^{tBu}bpy)_3]$ recorded from crystalline material dissolved in THF. Insets show simulated (red) and observed (black) isotopic envelopes for $[Al(^{tBu}bpy)_3]^+$, $[Al(^{tBu}bpy)_2]^+$, and $[Al(^{tBu}bpy)]^+$.

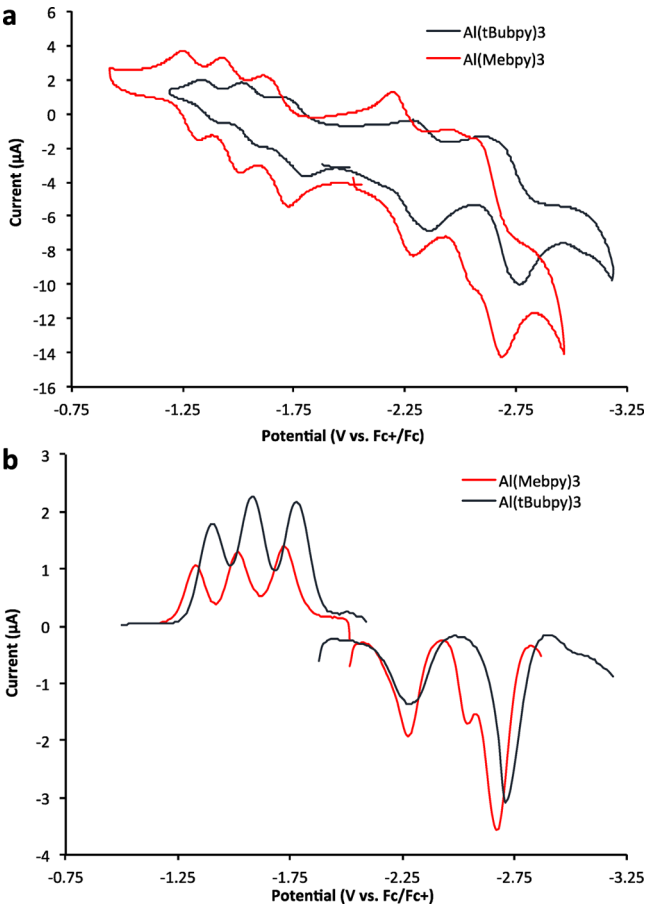

Figure 6. Cyclic voltammograms of (a) 2 mM $[Al(^{tBu}bpy)_3]$ (scan rate of 20 mV s^{-1}) and 2 mM $[Al(^{Me}bpy)_3]$ (scan rate of 20 mV s^{-1}) showing the near-reversible peaks. (b) Square-wave voltammograms of $[Al(^{tBu}bpy)_3]$ and $[Al(^{Me}bpy)_3]$ both recorded at a scan rate of 30 mV s^{-1} (red, oxidative processes; blue, reductive processes). All data were recorded at room temperature in CH_3CN solutions containing 0.1 M $[N(n\text{Bu})_4][PF_6]$. Potentials are referenced vs the Fc^+/Fc redox couple.

in $E_{1/2}$ values (ΔE) for the oxidations in both **1** and **2** are constant at ~0.20 V. In contrast the ΔE values for the reduction forms are more variable between the two complexes. These observations are further supported by the square-wave voltammograms collected for both **1** and **2** (Figure 6b).

The electrochemical behaviors of **1** and **2** are quite similar to Co(III) and Cr(III) complexes that have rich ligand-based electrochemistry with redox inactive M(III) centers.[52,53] For **1** and **2** the first three waves positive to the rest potential are attributed to one-electron oxidations of $[Al(^{R}bpy)_3]$ and the set of waves negative to the rest potential correspond to three successive one-electron reductions of **1** and **2**. The final reduction corresponding to the formation of $[Al^{3+}(^{tBu}bpy^{2-})_3]^{3-}$ is irreversible. Scheme 2 illustrates these electrochemical processes. These analyses suggest that the fully reduced forms, $[Al^{3+}(^{R}bpy)_3]^{3-}$, of both **1** and **2** are accessible.

Beyond the peaks representing the 2+/3+ couples, there are two additional irreversible oxidation waves for the both complex **1** (0.362 and 0.712 V) and complex **2** (0.313 and 0.662 V) that result in compound decomposition and precipitation of white powder.

The electronic coupling between the bpy redox centers can be evaluated through the analysis of comproportionation constant, K_c, defined by the representative equilibria shown in Scheme 3. The value of K_c can be calculated directly from the ΔE values according to eq 2.[54] When using the ΔE from the SWV experiments, we obtain K_c values of $10^{3.38}$ for the oxidations of **1** and **2**. The average ΔE values for the reductive events for **1** and **2** yield K_c values of $10^{5.92}$ and $10^{4.39}$, respectively.[54]

$$K_c = e^{(\Delta E)F/RT} \tag{2}$$

The observed K_c values associated with the oxidations are indicative of weakly or noncoupled electrochemical processes in complexes **1** and **2** (class I mixed-valent compounds) whereas the reductions appear to be more strongly electronically coupled (class II mixed-valent compounds). For reference, similar electrochemical studies performed on the related Al^{3+} bisiminopyridine complexes, specifically, $(IP^-)_2AlCl$ (IP = $N_2C_{18}H_{44}$), with N−N bidentate ligands show ΔE values for one-electron processes of 0.34 and 0.19 V corresponding to $K_c = 10^{5.8}$ and $K_c = 10^{3.21}$, respectively.[55] The former is associated with class II mixed-valent compounds, in which the bpy ligands are electronically coupled through the Al center. The latter process ($K_c = 10^{3.21}$) is associated with class I behavior indicative of virtually nonexistent coupling in these electrochemical events.[55]

Magnetic Properties. The magnetic properties of complexes **1** and **2** were measured in both the solid-state (dc susceptibility) and in solution (EPR, Evans method NMR). The dc susceptibilities of both complexes (Figure 7) show Curie−Weiss behavior and large, negative Weiss constants (−526 K for **1** and −437 K for **2**) associated with strong antiferromagnetic coupling. Fits of the high temperature data to the Curie−Weiss law (eq 3) are obtained with the following:

$$\chi = \frac{C}{(T - \theta)} \tag{3}$$

Here C is the Curie constant, and θ is the Weiss constant, giving effective magnetic moments of 3.78 μ_B (**1**) and 3.88 μ_B (**2**), which are indicative of $S = {}^3/_2$ spin states associated with the three unpaired electrons of the $(^{R}bpy^{\bullet})^{1-}$ radical anions. Below 140 K, the effective magnetic moment of **1** steadily decreases from 3.78 μ_B to 0.78 μ_B at 5 K. This behavior is consistent with the predicted $S = {}^1/_2$ ground state of the

DOI: 10.1021/acs.inorgchem.6b00034
Inorg. Chem. 2016, 55, 4344−4353

Table 5. Reduction Potentials ($E_{1/2}$, V) for Al(^{R}bpy)$_3$ Complexes and Ligands from SWV[a]

complex	3+/2+	2+/1+	1+/0	ΔE	0/1−	1−/2−	2−/3−	ΔE
[Al(^{tBu}bpy)$_3$]	−1.38	−1.58	−1.78	≈0.20	−2.30	−2.67	−3.00[b]	≈0.35
[Al(^{Me}bpy)$_3$]	−1.32	−1.52	−1.72	≈0.20	−2.28	−2.54[c]	−2.67	0.26[d]
^{tBu}bpy					−1.68	−2.71		≈1.03
^{Me}bpy					−1.66	−2.75		≈1.09

[a]Potentials were obtained from SWV measurements and are referenced versus the ferrocenium/ferrocene couple, Fc^+/Fc. [b]Irreversible. [c]The 1−/2− and 2−/3− $E_{1/2}$ values are estimated due to overlap. [d]Value based on difference between 0/1− and 1−/2− $E_{1/2}$ values due to poor separation of the 1−/2− and 2−/3− $E_{1/2}$ values.

Scheme 2. Complexes in the Electron Transfer Series for [Al(^{tBu}bpy)$_3$] (1) and [Al(^{Me}bpy)$_3$] (2)[a]

$$[Al^{III}(^{R}bpy)_3]^{3+} \overset{+e}{\underset{-e}{\rightleftharpoons}} [Al^{III}(^{R}bpy)_2(^{R}bpy^{\bullet})]^{2+} \overset{+e}{\underset{-e}{\rightleftharpoons}} [Al^{III}(^{R}bpy)(^{R}bpy^{\bullet})_2]^{+} \overset{+e}{\underset{-e}{\rightleftharpoons}} [Al^{III}(^{R}bpy^{\bullet})_3]$$
$$\overset{+e}{\underset{-e}{\rightleftharpoons}} [Al^{III}(^{R}bpy^{\bullet})_2(^{R}bpy^{2-})]^{-} \overset{+e}{\underset{-e}{\rightleftharpoons}} [Al^{III}(^{R}bpy^{\bullet})(^{R}bpy^{2-})]^{2-} \overset{+e}{\underset{-e}{\rightleftharpoons}} [Al^{III}(^{R}bpy^{2-})_3]^{3-}$$ **

[a]For Al(^{tBu}bpy)$_3$ the reduction from $[Al^{III}(^{R}bpy)_3]^{2-}$ to $[Al^{III}(^{R}bpy)_3]^{3-}$ is irreversible.

Scheme 3. Comproportionation (K_c) Processes for Reductive Species of 1 and 2

$$[Al(^{R}bpy)_3]^{0} + [Al(^{R}bpy)_3]^{2-} \overset{K_c}{\rightleftharpoons} 2[Al(^{R}bpy)_3]^{1-}$$
$$[Al(^{R}bpy)_3]^{1-} + [Al(^{R}bpy)_3]^{3-} \overset{K_c}{\rightleftharpoons} 2[Al(^{R}bpy)_3]^{2-}$$

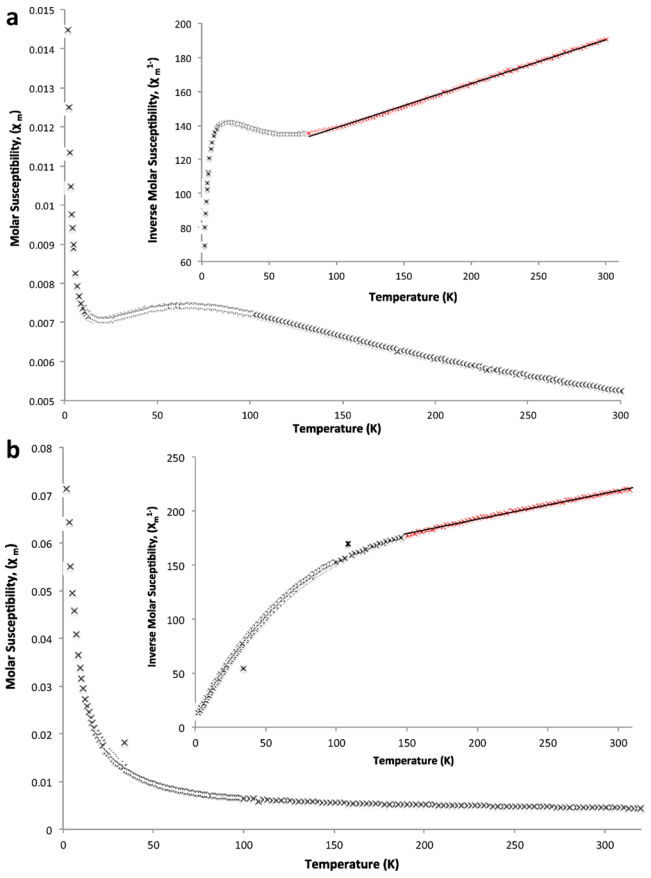

Figure 7. Molar magnetic susceptibility as a function of temperature of (a) [Al(^{tBu}bpy)$_3$] and (b) [Al(^{Me}bpy)$_3$]. Insets show the reciprocal susceptibility versus temperature in which the red data represent the Curie−Weiss regions and the solid black lines are the fits to eq 3.

Al(bpy)$_3$ complexes and the presence of low lying $S = {}^3/_2$ excited states that are populated at room temperature.

In addition to the strong antiferromagnetic coupling within the Al(^{R}bpy)$_3$ complexes, crystals of **2** appear to show weak 3-D antiferromagnetic interactions below 90 K as indicated by the deviation from C−W behavior and the suppression of the magnetic moments prior to the appearance of a Curie tail. The behavior is similar to that observed for the M(C$_2$(CN)$_4$)-[C$_4$(CN)$_8$]$_{1/2}$ complexes (M = Mn, Fe)[56] although additional magnetic studies are necessary to fully understand the magnetic properties of **2**.

The magnetic moments of the Al(^{R}bpy)$_3$ complexes were also measured in solution via the Evans NMR method (see Experimental Details). The measured moment for **1** in CH_3CN (1.73 μ_B) is equal to the expected spin-only moment for an $S = {}^1/_2$ system. The moment for **2** is somewhat low (1.39 μ_B), presumably due to its limited solubility and associated errors of concentrations. The magnetic moments are unchanged when supporting electrolyte (0.1 M of [N(*n*-Bu)$_4$]PF$_6$ in CH_3CN) was added to the solution. While the Evans method studies of both complexes show strong paramagnetism in acetonitrile solutions, the room temperature susceptibilities are indicative of $S = {}^1/_2$ spin states, which is in sharp contrast to the room temperature solid-state $S = {}^3/_2$ spin states measured from the dc susceptibility studies described above.

The X-band EPR spectrum of **1** and **2** in THF at room temperature are similar to that reported for [Al(bpy)$_3$]^0 (**3**), with $g_{iso} \approx 2.0064$, and are consistent with $S = {}^1/_2$ systems in solution.

DFT Studies. Density functional theory calculations were performed using the B3LYP functional with a def2-TZVP basis set for all atoms, previously shown by Weighardt et al. to provide accurate structural properties and spin exchange coupling constants for [M(bpy)$_3$]^n compounds.[18] The exchange coupling parameters J were calculated using Yamaguchi's approximation[57]

$$J = -\frac{E_{HS} - E_{LS}}{\langle S^2\rangle_{HS} - \langle S^2\rangle_{LS}}$$

for each of the isolated Al(^{R}bpy)$_3$ structures. Here HS and LS denote the high and low spin state values of the DFT energies E and the spin-squared operator. This methodology is consistent with the approach taken by Wieghardt et al.[18,32] on related tris-bpy complexes. The results for R = H, Me, and *t*-Bu all indicate an $S = {}^1/_2$ ground state with a low lying $S = {}^3/_2$ excited state approximately 10 meV above the ground state (Table 6). Broken symmetry and unrestricted Kohn−Sham calculations on the $S = {}^1/_2$ state both converged to an identical electronic structure. In the ground state, two $(bpy^{\bullet})^{1-}$ radical anions are coupled antiferromagnetically. The third unpaired electron resides in a higher-lying ligand-based π^* orbital. To verify the validity of our approach, calculations were performed on [Al(bpy)$_3$] (**3**) and the results compared to those in the literature.[18] Table S3 shows a comparison of numerical data,

DOI: 10.1021/acs.inorgchem.6b00034
Inorg. Chem. 2016, 55, 4344−4353

Table 6. Spin Exchange Coupling Constants (J) and Spin State Energy Differences for $[Al^{III}(^{Me}bpy^{\bullet})_3]^0$ and $[Al^{III}(^{tBu}bpy^{\bullet})_3]^0$

complex	J_{calc} (cm^{-1})	$E_{1/2} - E_{3/2}$ [a,b] (meV)	θ [c] (K)	T_{CW} [d] (K)
$Al(bpy)_3$ (**3**)	−53.15	13.4	−667 [e]	∼160 [c]
$Al(^{Me}bpy)_3$ (**2**)	−35.33	8.9	−427	90
$Al(^{tBu}bpy)_3$ (**1**)	−40.27	10.1	−526	140

[a] $E_{1/2}$ = ground state energy. The $S = {}^1/_2$ state is the ground state in all cases. [b] $E_{3/2}$ = excited state energy. [c] Weiss constant (θ) from eq 3. [d] Temperature onset for high temperature Curie−Weiss behavior. [e] Data from ref 16.

and Figure S4 compares the calculated structures, which are in good agreement. In addition, the calculated bond distances (Table S4) are in excellent agreement with the experimental parameters (Table 6).

The calculated and observed J values are given in Table 6 and are in excellent agreement with the magnetic data described above. A strong correlation between all experimental and computational measurements is seen: in each case, the trend **2** < **1** < **3** is observed for experimental and computational values of J, $E_{3/2} - E_{1/2}$, and T_{CW}.

The molecular orbitals for $[Al(^{Me}bpy)_3]$ (**2**) in the $S = {}^1/_2$ ground state are given in Figure 8 and are constructed assuming

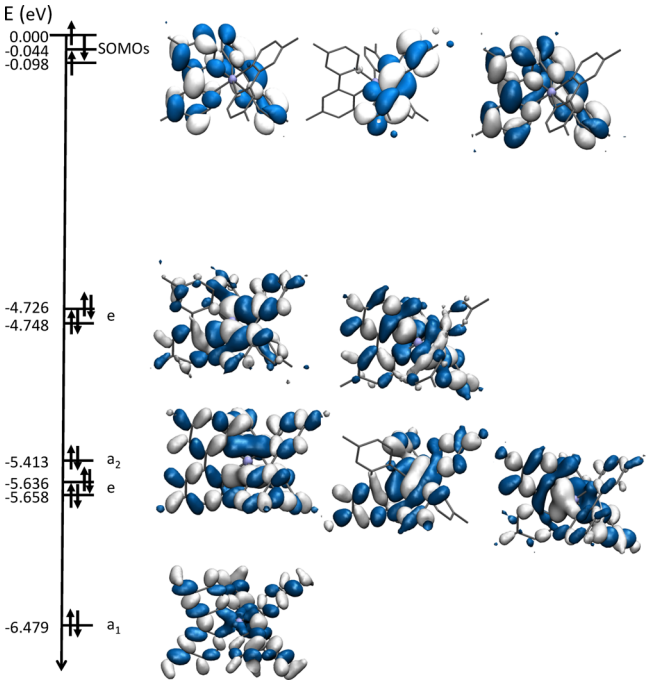

Figure 8. Frontier molecular orbitals in complex **2**. Lower energy orbitals for Al−N bonds. Antiferromagentically coupled SOMO orbitals are significantly higher in energy.

an idealized D_3 point symmetry. The three frontier orbitals in **2** are ligand-based and are π^* in character; this is in agreement with the electrochemical data and with previously reported studies. The MO diagram for **1** is similar. The energies of the three frontier, singly occupied orbitals are very close in energy. Antiferromagnetic coupling in **1** and **2** results in an $S = {}^1/_2$ ground state consistent with magnetometry data for both **1** and **2**.

DISCUSSION

Disproportionation reactions of $AlBr{\cdot}NEt_3$ in the presence of ^{R}bpy (R = Me or tBu) produce good yields of the homoleptic tris-bpy complexes $Al(^{tBu}bpy)_3$ (**1**) and $Al(^{Me}bpy)_3$ (**2**). Complexes **1** and **2** represent the first structurally characterized Al tris-bipyridyl complexes and the first main-group homoleptic tris-bipyridyl complexes containing monoanionic bpy ligands. The synthesis of these complexes differs from that of the analogous complex $Al(bpy)_3$ (**3**), which was synthesized from the reaction of $AlCl_3$ with $LiAlH_4$ in the presence of neutral bpy ligands. This difference in synthetic approach perhaps accounts for our ability to isolate these compounds in pure form. Both **1** and **2** exhibit the prototypical D_3 point symmetry common to $M(bpy)_3$ complexes. The structural, electrochemical, and magnetic properties along with the DFT studies for both compounds are indicative of complexes containing $(^Rbpy^{\bullet})^{1-}$ radical anions coordinated to Al^{3+} metal ions and confirm the structural predictions for **3**.[18,32]

Complexes **1** and **2** were prepared utilizing the disproportion pathway characteristic of metastable AlX·L (X = Cl or Br; L = donor solvent) solutions. Similar low valent Ga(I) starting materials have been previously applied to the synthesis of $[Ga(bpy)_3]^{3+}$ (**4**) and $[Ga(bpy)_3]^{2+}$ (**5**); however, the Ga complexes contain either all neutral bpy ligands (for **4**) or two neutral bpy ligands and one $(bpy^{\bullet})^{1-}$ radical anion (for **5**). With the characterization of **1** and **2**, aluminum now represents the only main-group metal in which complexes containing all three bpy redox states have been isolated and structurally characterized: $(bpy)^0$, $(bpy^{\bullet})^-$, and $(bpy)^{2-}$.[47,48] In addition, the structural data described here show that the intrachelate bond distance (C_{py}−C_{py}) is an excellent structural indicator of bpy oxidation state in main-group complexes, as established by Wieghardt and co-workers.

The properties of the $Al(^Rbpy)_3$ complexes show consistent trends in electronic and magnetic structures. First, both **1** and **2** are in the $S = {}^1/_2$ spin states at room temperature in solution, but in the solid-state, they exist in the $S = {}^3/_2$ excited states at room temperature. These data suggest that the solvation of the complexes either stabilizes the ground state or destabilizes the excited state (or both) relative to the solid-state complexes. Such a scenario is also consistent with the class II type electrochemical behavior in which the ligand-based spins show modest coupling through the Al centers in solution.[14,15] Second, the calculated and observed magnetic data also show consistent trends across the series of compounds. The calculated J values describing the spin exchange coupling decrease according to **2** < **1** < **3**, which directly correlates with the onset of Curie−Weiss behavior (T_{CW}) the Weiss constants (θ) shown in Table 6. For example, the lowest calculated J coupling is observed for **3**, which facilitates the unpairing of spins at a lower temperature ($S = {}^1/_2$ to $S = {}^3/_2$ spin transition) and a larger $S = {}^3/_2$ Curie−Weiss region. These data are also in excellent agreement with the calculated differences in energy between the $S = {}^1/_2$ and $S = {}^3/_2$ spin states ($E_{1/2} - E_{3/2}$).

The electrochemistry of both **1** and **2** demonstrate that six additional oxidation states of the complexes are accessible from the neutral species: $[Al(^Rbpy)_3]^{3+}$, $[Al(^Rbpy)_3]^{2+}$, $[Al(^Rbpy)_3]^{1+}$, $[Al(^Rbpy)_3]^{1-}$, $[Al(^Rbpy)_3]^{2-}$, $[Al(^Rbpy)_3]^{3-}$. These interconversions occur through a series of single electron oxidations and reductions. The oxidation processes occur through the addition and removal of electrons from the singly occupied ligand-based π^* molecular orbitals (SOMO) of the

DOI: 10.1021/acs.inorgchem.6b00034
Inorg. Chem. 2016, 55, 4344−4353

$(bpy^{\bullet})^{-}$ ligands (Figure 8). The reduction processes observed for both **1** and **2** are weakly coupled through the ligand-based orbitals and the aluminum center, as indicated by the comproportionation constants, K_c, of $10^{5.92}$ and $10^{4.39}$.

Previous studies of **3** demonstrated that antiferromagnetic interactions give rise to a ground state doublet that is slightly more stable than the low lying quartet excited state, with a gap of 230−240 cm^{-1} ($-3\,J/k_B$ = 330−345 K).[58] For reference, the scandium analogue's gap is 420 cm^{-1} ($-3\,J/k_B$ = 600 K).[58] In **3** these two states are extremely close in energy. Theoretical studies have shown that the $S = {}^1/_2$ ground state is attained through an intramolecular antiferromagnetic exchange coupling between two of the $(bpy^{\bullet})^{-}$ anions through the diamagnetic central metal ion. These exchange pathways are available because the $(bpy^{\bullet})^{-}$ anions are not orthogonal to one another.[32]

Both **1** and **2** show similar antiferromagnetic coupling below 130 K (**1**) and 80 K (**2**), respectively, consistent with the expected $S = {}^1/_2$ ground state. Above these temperatures the data show $S = {}^3/_2$ spin states that are indicative of thermally populated low lying quartet excited states with three unpaired electrons. This behavior is similar to that of **3**; however, the magnetic properties differ at lower temperatures: the antiferromagnetic coupling below 40 K in **1** gives rise to an effective moment of 0.78 μ_B, less than half of what would be expected for a spin $^1/_2$ system. At this point, we speculate that this difference in ground state behavior is a result of intermolecular interactions that further reduce the magnetic moment.

The low temperature magnetic data for **2** is even more unusual in that it shows an apparent long-range ordering below 80 K. While long-range ordering is ubiquitous in solid-state chemistry, magnetic ordering between discrete molecules above 10 K is not common.[59] Similar interpretations for the magnetic data of $[Ru(bpy)_3]^0$ have been proposed for extremely broad "sub-Curie" tail displayed by this compound.[60] More recently it has been reported that the spins of the two $(bpy^{\bullet})^{-}$ radicals in $[Ru^{II}(bpy^{\bullet})_2(bpy^0)]$ are strongly antiferromagnetically coupled to one another. The observed coupling is through the diamagnetic Ru^{II} center and not intermolecular in nature due to suboptimal $\pi-\pi$ contacts, resulting in a diamagnetic ground state ($S = 0$) and excited triplet state ($S = 1$).[32] It is our belief that our narrower "sub-Curie" tail in **2** may be the result of intermolecular interactions between the bpy ligands due to the presence of $\pi-\pi$ stacking. This stacking, in concert with the closeness in energy between the ground and excited state due to the Al center, results in the unexpected "ordering" observed at low temperatures. Further studies of this system are in progress.

CONCLUSION

The reactions of substituted bpy ligands with the metastable AlX precursors (X = Br, Cl) produce crystalline homoleptic tris-bpy complexes **1** and **2** in good yields. These compounds represent the first structurally characterized homoleptic tris-bpy Al complexes. With the report of **1** and **2**, aluminum is one of the only metals to have structurally characterized derivatives of all three oxidation states of bpy-type ligands: $[Al^{III}Cl_2(bpy^0)_2]$-$Cl{\cdot}CH_3CN$,[48] $[Al^{III}(^{R}bpy^{\bullet})^{1-}_3]$ (where R = Me_2 or tBu_2), and $[Li^+(THF)_4][Al^{III}(bpy^{2-})_2]^-$.[47] The related $[Ga(bpy)_3]^{3+/2+}$ complexes[7,8] also contain Ga^{3+} central metal ion but have either all neutral or predominantly neutral bpy ligands. Interestingly, both the Al^{3+} and Ga^{3+} series of complexes were both formed from M^{+1} precursors.

Both complexes **1** and **2** display $S = {}^1/_2$ ground states and low lying $S = {}^3/_2$ excited states, similar to those previously reported for $Al(bpy)_3$. In solution, **1** and **2** reside in their $S = {}^1/_2$ ground state, which presumably results from solvent stabilization of the ground state, destabilization of the excited state, or both. In **2** there is apparent long-range magnetic ordering in the solid-state below 80 K, which has not been reported in similarly ligated transition-metal methyl bpy complexes.

The solution electrochemical properties of **1** and **2** are similar and show that it may be possible to isolate other oxidation states of these complexes. To date, this is the most complete report of a main-group centered homoleptic tris-bpy complex.

EXPERIMENTAL DETAILS

General Considerations. All air- and water-free manipulations were performed using standard Schlenk techniques or in an argon-filled glovebox. Solvents were dried over proper drying agents according to literature procedures: toluene, THF, and hexane were distilled over sodium benzophenone and triethylamine over calcium hydride. Bipyridyl (bpy), 4-4′-di-*tert*-butyl-2,2′-bipyridine (^{tBu}bpy), and 4-4′-dimethyl-2,2′-bipyridine (^{Me}bpy) were purchased from Sigma-Aldrich and dried *in vacuo* before use.

$AlBr{\cdot}(NEt_3)_n$. Aluminum metal (0.5514 g, 20.4 mmol) was reacted with gaseous HBr (24.29 mmol) over 3 h at approximately 1200 K in a modified Schnöckel-type metal halide co-condensation reactor. The resultant gas-phase AlBr was co-condensed with a mixture of toluene/triethylamine (3:1 v/v) at approximately 77 K. The solvent matrix was thawed to −80 °C and the resultant yellow-brown solution stored at that temperature prior to use. Titration of the $AlBr{\cdot}(NEt_3)_n$ via Mohr's method determined a bromide concentration of 152 mM and Al/Br ratio of 1:1.19.

$AlCl{\cdot}(Et_2O)_n$. Aluminum metal (0.5514 g, 20.4 mmol) was reacted with gaseous HCl (37.28 mmol) over 3 h at approximately 1200 K in a modified Schnöckel-type metal halide co-condensation reactor. The resultant gas-phase AlBr was co-condensed with a mixture of toluene/diethyl ether (3:1 v/v) at approximately 77 K. The solvent matrix was thawed to −80 °C and the resultant yellow-brown solution stored at that temperature prior to use. Titration of the $AlCl{\cdot}(Et_2O)_n$ via Mohr's method determined a chloride concentration of 187 mM and Al/Cl ratio of 1:1.25.

$[Al(^{tBu}bpy)_3]$ (1) [Method A]. THF (15 mL) was added to a 50 mL Schlenk vessel containing ^{tBu}bpy (0.4310 g; 1.61 mmol). The ^{tBu}bpy was dissolved, resulting in a clear colorless solution, to which $AlBr{\cdot}(NEt_3)_n$ (1.61 mmol, 10.6 mL of a 152 mM solution in toluene/triethylamine 3:1) was added via syringe at room temperature. The dark green reaction mixture was stirred for 12 h and subsequently concentrated *in vacuo* to ∼10 mL, filtered via cannula, and stored at room temperature. After a period of 3 days, dark green needles crystallized from the reaction mixture (total yield 35%).

$[Al(^{tBu}bpy)_3]$ [Method B]. $AlCl{\cdot}(Et_2O)_n$ (0.5 mmol, 2.2 mL of a 233 mM solution in toluene/diethyl ether 3:1) was added via syringe at room temperature to a Schlenk vessel charged with ^{tBu}bpy (0.1340 g; 0.5 mmol). The dark green reaction mixture was stirred for 1 h at room temperature and subsequently concentrated under vacuum to $^3/_4$ of its original volume, filtered via cannula, and stored at room temperature for 1 week. The reaction mixture was then transferred to a vial in a glovebox and subsequently layered with hexane. After 3 weeks, large dark green crystals formed on the walls of the vial. Preliminary structure analysis supports the formation of $[Al(^{tBu}bpy)_3]$.

$[Al(^{Me}bpy)_3]$ (2). THF (15 mL) was added to a 50 mL Schlenk vessel containing ^{Me}bpy (0.3721 g; 2 mmol). The ^{Me}bpy was dissolved, resulting in a clear solution, to which $AlBr{\cdot}(NEt_3)_n$ (2 mmol, 13.2 mL of a 152 mM solution in toluene/triethylamine 3:1) was added via

DOI: 10.1021/acs.inorgchem.6b00034
Inorg. Chem. 2016, 55, 4344−4353

syringe at room temperature. The dark pink-red reaction mixture was stirred for 12 h and subsequently concentrated under vacuum to $^3/_4$ its original volume, filtered via cannula, and stored at room temperature. After a period of 3 days, black needles crystallized from the reaction mixture (total yield 36%).

Physical Methods. *Single-Crystal Data.* Crystallographic data was collected on Bruker Smart Apex2 diffractometer using graphite monochromated Mo Kα radiation (λ = 0.710 73 Å) and CCD detector. Data were corrected for absorption effects using multiscan methods; the structure was solved and refined using the Bruker ShelXTL software.

Powder X-ray Diffraction (XRD). The XRD pattern for **1** was obtained on a Bruker D8 Advance diffractometer equipped with LynxEye detector using a monochromatic Cu Kα radiation source biased at 40 kV and 40 mA. A dome supplied by Bruker was used to ensure air-free characterization of **1**. The XRD pattern of **2** was obtained on a Bruker C2 Discover diffractometer equipped with a VÅNTEX-500 detector using a monochromatic Cu Kα radiation source biased at 40 kV and 40 mA. For air-free collection, **2** was loaded into a 0.7 mm glass capillary and sealed with epoxy. The XRD patterns were background corrected. Experimental and calculated powder XRD data can be found in the Supporting Information.

Evans Method Experiments. Two Evans method experiments were performed on a 500 MHz Bruker instrument: one with a CH_3CN solvent/standard and another in CH_3CN containing 0.1 M $[N(n\text{-}Bu)_4]PF_6$ as solvent/standard. See Supporting Information for experimental details.

Electrochemical Measurements. Measurements utilized a Pine WaveNow potentiostat inside a glovebox under Ar atmosphere. The electrochemical cell consisted of a modified three-electrode setup with a glassy carbon working electrode, a platinum counter electrode, and a silver wire pseudoreference electrode. Ferrocene was used as an internal reference and introduced at the end of the experiment. All potentials are referenced to the Fc^+/Fc couple.

Zero Field Cooled Magnetometry. Superconducting quantum interference device (SQUID) magnetization data of crystalline samples were recorded with a SQUID magnetometer at 1 T.

ESI-MS. Positive ion electrospray mass spectra of **1** and **2** were collected on an ACCUTOF ESI-MS operating at 3000 V in THF solution. Samples were injected utilizing an air-free ionization source.

■ ASSOCIATED CONTENT

Supporting Information

The Supporting Information is available free of charge on the ACS Publications website at DOI: 10.1021/acs.inorgchem.6b00034.

Crystallographic data for **1** (CIF)
Crystallographic data for **2** (CIF)
Characterization data (PDF)

■ AUTHOR INFORMATION

Corresponding Author

*E-mail: eichhorn@umd.edu.

Notes

The authors declare no competing financial interest.

■ ACKNOWLEDGMENTS

We thank DTRA (HDTRA-1-12-1-007) for support of this research. We thank Mr. Xiuquan Zhou and Prof. Efrain Rodriguez for collection of the magnetic data and helpful discussions.

■ REFERENCES

(1) Kaes, C.; Katz, A.; Hosseini, M. W. *Chem. Rev.* **2000**, *100*, 3553−3590.
(2) Perez-Cordero, E.; Buigas, R.; Brady, N.; Echegoyen, L.; Arana, C.; Lehn, J.-M. *Helv. Chim. Acta* **1994**, *77*, 1222−1228.
(3) Scarborough, C. C.; Wieghardt, K. *Inorg. Chem.* **2011**, *50*, 9773−9793.
(4) Bowman, A. C.; Sproules, S.; Wieghardt, K. *Inorg. Chem.* **2012**, *51*, 3707−3717.
(5) Wang, M.; Weyhermüller, T.; England, J.; Wieghardt, K. *Inorg. Chem.* **2013**, *52*, 12763.
(6) Pérez Cordero, E. E.; Campana, C.; Echegoyen, L. *Angew. Chem., Int. Ed. Engl.* **1997**, *36*, 137−140.
(7) Baker, R. J.; Jones, C.; Kloth, M.; Mills, D. P. *New J. Chem.* **2004**, *28*, 207.
(8) Lichtenthaler, M. R.; Stahl, F.; Kratzert, D.; Heidinger, L.; Schleicher, E.; Hamann, J.; Himmel, D.; Weber, S.; Krossing, I. *Nat. Commun.* **2015**, *6*, 8288.
(9) Wulf, E.; Herzog, S. *Z. Anorg. Allg. Chem.* **1972**, *387*, 81−90.
(10) England, J.; Wieghardt, K. *Inorg. Chem.* **2013**, *52*, 10067−10079.
(11) Suthar, B.; Aldongarov, A.; Irgibaeva, I. S.; Moazzen, M.; Donovan-Merkert, B. T.; Merkert, J. W.; Schmedake, T. A. *Polyhedron* **2012**, *31*, 754−758.
(12) Ma, G.; Kritikos, M.; Maliarik, M.; Glaser, J. *Inorg. Chem.* **2004**, *43*, 4328−4340.
(13) Robinson, G. H. *Coordination Chemistry of Aluminum*; VCH Publishers, 1993.
(14) Larsen, S. C.; Braddock-Wilking, J.; Farrar, C. T.; Leman, J. T.; Singel, D. J.; Barron, A. R. *J. Am. Chem. Soc.* **1995**, *117*, 1746−1753.
(15) Braddock-Wilking, J.; Leman, J. T.; Farrar, C. T.; Cosgrove-Larsen, S. A.; Singel, D. J.; Barron, A. R. *J. Am. Chem. Soc.* **1995**, *117*, 1736−1745.
(16) Inoue, M.; Horiba, T.; Hara, K.-I. *Bull. Chem. Soc. Jpn.* **1978**, *51*, 3073−3074.
(17) Herzog, S.; Geisler, K.; Präkel, H. *Angew. Chem., Int. Ed. Engl.* **1963**, *2*, 47.
(18) Bowman, A. C.; England, J.; Sproules, S.; Weyhermüller, T.; Wieghardt, K. *Inorg. Chem.* **2013**, *52*, 2242−2256.
(19) Tacke, M.; Schnöckel, H. *Inorg. Chem.* **1989**, *28*, 2895−2896.
(20) Herzog, S.; Grimm, U. *Z. Chem.* **1968**, *8*, 186−187.
(21) Herzog, V. S.; Gustav, K.; Schuster, R. *Z. Naturforsch., B: J. Chem. Sci.* **1962**, *15b*, 67.
(22) Herzog, S.; Taube, R. *Z. Anorg. Allg. Chem.* **1960**, *306*, 159−179.
(23) Albrecht, G. *Z. Chem.* **1963**, *3*, 182−187.
(24) Herzog, V. S.; Zühlke, H. *Z. Naturforsch., B: J. Chem. Sci.* **1960**, *15*, 466.
(25) Quirk, J.; Wilkinson, G. *Polyhedron* **1982**, *1*, 209.
(26) Brandt, W. W.; Dwyer, F. P.; Gyarfas, E. D. *Chem. Rev.* **1954**, *54*, 959−1017.
(27) Herzog, V. S.; Renner, K. C.; Schön, W. *Z. Naturforsch., B: J. Chem. Sci.* **1957**, *12b*, 809.
(28) Herzog, S.; Schneider, I. *Z. Chem.* **1962**, *2*, 24−24.
(29) Herzog, S.; Präkel, H. *Z. Chem.* **1965**, *5*, 469−470.
(30) Hall, F. S.; Reynolds, W. L. *Inorg. Chem.* **1966**, *5*, 931−932.
(31) Herzog, S.; Klausch, U.; Lantos, J. *Z. Chem.* **1964**, *4*, 150−150.
(32) England, J.; Scarborough, C. C.; Weyhermüller, T.; Sproules, S.; Wieghardt, K. *Eur. J. Inorg. Chem.* **2012**, *2012*, 4605−4621.
(33) Wang, M.; England, J.; Weyhermüller, T.; Wieghardt, K. *Inorg. Chem.* **2014**, *53*, 2276−2287.
(34) van Albada, G. A.; Mutikainen, I.; Turpeinen, U.; Reedijk, J. *Acta Crystallogr., Sect. E: Struct. Rep. Online* **2005**, *E61*, m1411−m1412.
(35) Amarante, T. R.; Fernandes, J. A.; Gonçalves, I. S.; Almeida Paz, F. A. *Acta Crystallogr., Sect. E: Struct. Rep. Online* **2011**, *E67*, m1828−m1829.
(36) Lehleh, A.; Beghidja, A.; Beghidja, C.; Mentré, O.; Welter, R. *C. R. Chim.* **2011**, *14*, 462−470.
(37) Han, Z.-G.; Li, S.; Wu, J.-J.; Zhai, X.-L. *J. Coord. Chem.* **2011**, *64*, 1525−1532.
(38) Huang, W.; Qian, H. *Transition Met. Chem.* **2006**, *31*, 621−629.
(39) Schwalbe, M.; Schäfer, B.; Görls, H.; Rau, S.; Tschierlei, S.; Schmitt, M.; Popp, J.; Vaughan, G.; Henry, W.; Vos, J. G. *Eur. J. Inorg. Chem.* **2008**, *2008*, 3310−3319.

DOI: 10.1021/acs.inorgchem.6b00034
Inorg. Chem. 2016, 55, 4344−4353

(40) Sandroni, M.; Zysman-Colman, E. *Dalton. Trans.* **2014**, *43*, 3676.
(41) Li, J.-H.; Wang, J.-T.; Zhang, L.-Y.; Chen, Z.-N.; Mao, Z.-W.; Ji, L.-N. *Inorg. Chim. Acta* **2009**, *362*, 1918−1924.
(42) Yang, X.-J.; Wu, B.; Janiak, C. *CrystEngComm* **2004**, *6*, 126.
(43) Rutherford, T. J.; Pellegrini, P. A.; Aldrich Wright, J.; Junk, P. C.; Keene, F. R. *Eur. J. Inorg. Chem.* **1998**, *1998*, 1677−1688.
(44) Damrauer, N. H.; Boussie, T. R.; Devenney, M.; McCusker, J. K. *J. Am. Chem. Soc.* **1997**, *119*, 8253−8268.
(45) Zhang, Y.; Zhou, N.; Akella, S.; Kuang, Y.; Kim, D.; Schwartz, A.; Bezpalko, M.; Foxman, B. M.; Fraden, S.; Epstein, I. R. *Angew. Chem., Int. Ed.* **2013**, *52*, 11494−11498.
(46) Yadav, Y. J.; Mastropietro, T. F.; Szerb, E. I.; Talarico, A. M.; Pirillo, S.; Pucci, D.; Crispini, A.; Ghedini, M. *New J. Chem.* **2013**, *37*, 1486.
(47) Nikiforov, G. B.; Roesky, H. W.; Noltemeyer, M.; Schmidt, H.-G. *Polyhedron* **2004**, *23*, 561−566.
(48) Bellavance, P. L.; Corey, E. R.; Corey, J. Y.; Hey, G. W. *Inorg. Chem.* **1977**, *16*, 462−467.
(49) Scarborough, C. C.; Sproules, S.; Weyhermüller, T.; DeBeer, S.; Wieghardt, K. *Inorg. Chem.* **2011**, *50*, 12446−12462.
(50) Martinez, C. R.; Iverson, B. L. *Chem. Sci.* **2012**, *3*, 2191.
(51) Janiak, C. *J. Chem. Soc., Dalton Trans.* **2000**, 3885−3896.
(52) Chun, H.; Verani, C. N.; Chaudhuri, P.; Bothe, E.; Bill, E.; Weyhermüller, T.; Wieghardt, K. *Inorg. Chem.* **2001**, *40*, 4157−4166.
(53) Taube, H. *Chem. Rev.* **1952**, *50*, 69−126.
(54) D'Alessandro, D. M.; Keene, F. R. *Dalton Trans.* **2004**, 3950.
(55) Myers, T. W.; Kazem, N.; Stoll, S.; Britt, R. D.; Shanmugam, M.; Berben, L. A. *J. Am. Chem. Soc.* **2011**, *133*, 8662−8672.
(56) McConnell, A. C.; Shurdha, E.; Bell, J. D.; Miller, J. S. *J. Phys. Chem. C* **2012**, *116*, 18952−18957.
(57) Soda, T.; Kitagawa, Y.; Onishi, T.; Takano, Y.; Shigeta, Y.; Nagao, H.; Yoshioka, Y.; Yamaguchi, K. *Chem. Phys. Lett.* **2000**, *319*, 223−230.
(58) Kobayashi, H.; Kaizu, Y.; Matsuzawa, H.; Sekino, H.; Torii, Y. *Mol. Phys.* **1993**, *78*, 909−928.
(59) Goβ, K.; Gatteschi, D.; Bogani, L. *Phys. Chem. Chem. Phys.* **2014**, *16*, 18076−18082.
(60) Wagner, M. J.; Dye, J. L.; Perez-Cordero, E.; Buigas, R.; Echegoyen, L. *J. Am. Chem. Soc.* **1995**, *117*, 1318−1323.

DOI: 10.1021/acs.inorgchem.6b00034
Inorg. Chem. 2016, 55, 4344−4353